ELSEVIER

International Journal of Solids and Structures 41 (2004) 1021–1037

INTERNATIONAL JOURNAL OF SOLIDS and STRUCTURES

www.elsevier.com/locate/ijsolstr

Comparison of computational predictions of material failure using nonlocal damage models

Huang Yuan [a,*], Jian Chen [b]

[a] MTU Aero Engine GmbH, MTPV, Dachauer Str. 665, D-80995 Munich, Germany
[b] Alstom Power (Schweiz) AG, CH-5401 Baden, Switzerland

Received 3 December 2002; received in revised form 14 August 2003

Abstract

In computational analysis of damage failure the strain delocalizations are of great importance in predicting assessment of structure integrity. In this paper we are investigating effects of the intrinsic material length on computational prediction of material failure using both cell model, i.e. the conventional micro-mechanical damage model with the constant–sized finite elements for the damage zones, and nonlocal damage model based on the gradient plasticity. The corresponding experiments performed for an engineering steel are taken as reference for verification. The experimental observation has revealed that reducing the specimen size will arise the specific strength of small notched specimen which cannot be predicted using the cell damage model. The nonlocal damage model based on the strain gradient-dependent constitutive plasticity theory reproduces the experimental records. The material length affects evolution of the material porosity and gives an understandable explanation of the size effect.

Keywords: Size effects; Micro-mechanical damage model; Gradient plasticity; Ductile material failure; Intrinsic material length; Finite element method

1. Introduction

Ductile material failure is characterized by the micro-void nucleation, growth and coalescence mechanism. The damage model (GTN model), originally introduced by Gurson (1977) and modified by Tvergaard and Needleman (Tvergaard, 1981; Tvergaard and Needleman, 1984), is attractive since it is not derived from purely heuristic arguments, but from micro-mechanical analysis. The yield function of the GTN model accounts for voids in terms of one single internal variable, i.e. the void volume fraction or the porosity. A micro-void initiates and grows due to high plastic strains or high stress triaxiality (Chu and Needleman, 1980). One may imagine that the initiation and propagation of the micro-void depend on both amplitude and distribution of the equivalent plastic strain as well as the stress triaxiality in the vicinity of the micro-void. It means that the evolution of material damage is practically a nonlocal process. These

* Corresponding author. Tel.: +49-891489-9294; fax: +49-891489-2728.
E-mail address: huang.yuan@muc.mtu.de (H. Yuan).

0020-7683/$ - see front matter © 2003 Elsevier Ltd. All rights reserved.
doi:10.1016/j.ijsolstr.2003.09.017

observations imply that there is a need for such micro-mechanical approach to incorporate an intrinsic material length parameter into the constitutive relation (Hutchinson, 2000).

Nonlocal forms of the GTN model in which the strain delocalization is realized by delocalization the damage variable, i.e. the porosity, have been developed by Leblond et al. (1994), Tvergaard and Needleman (1995) and so on. The basic idea is that the effect and evolution of the porosity should be changed in order to eliminate the strain localization because the matrix itself is described by the stable Mises plasticity. The porosity will be averaged in a small neighboring region. From numerical point of view, such approach is similar to the technique to fit a constant-sized finite elements to the material micro-structure (Brocks et al., 1995; Xia and Shih, 1995), in which the size of the so-called cell elements is chosen to be representative of the mean spacing between voids. It follows that each cell element contains a single void at the initial volume fraction (Xia and Shih, 1995). Growth and coalescence of the void is related to the stress and strain averaged over the cell element.

Physically it is argued that the micro-mechanical behaviour cannot be described by the continuum mechanics on which the finite element method is based. The cell element is taken as the smallest cell which can be resolved using the continuum mechanics. From fracture energy point of view the fracture energy dissipation in a finite element is proportional to its size. The constant sized element limits the energy dissipation for crack growth. It seems to be a kind of regulation of the porosity distribution. In comparison with the treatments in Leblond et al. (1994) and Tvergaard and Needleman (1995), the cell element method is a straight way for averaging and very simple for finite element computations. One does not need any changes in his finite element code to start such simulations. Its application is, however, restricted to crack analysis in small sized specimens due to increasing computational efforts. In crack tip fields effects of the element size become essential due to extremely high stress and strain gradients. Varying the element size may significantly changes the damage zone. Furthermore, there are no systematic study available to examine the interaction of the cell element size and the local damage evolution, at least in notched specimens. Interdependence of the cell element size with the strain gradients which vary with the notch radius remains an open issue.

The additional explanation why one has to use the constant element size is that the smallest element size should be larger than the void space. The GTN model homogenizes the small representative material volume containing a micro-void and, therefore, the smallest element size has to be larger than the smallest representative material volume. According to our opinion such explanations confuses the concept of a physical model with the numerical method, e.g. the finite element method. The homogenized representative material volume is described by continuum mechanics equations including the special constitutive equations. The finite element method is a numerical method to solve the field governing equations. If the governing equations are well-conditioned, the finite element method does yield a more accurate solution by using finer finite elements. The finite elements are certainly not related to the representative material volume, but the accuracy of numerical solution. One may not expect to find the true solution for the representative material volume by using one linear or quadratic interpolation of the displacement vector. The numerical solution obtained from a certainly sized element mesh cannot be the accurate solution for the damage problem, but an approximation. Since the present problem is so ill-conditioned that the numerical solutions substantially vary the element size. Why this occurs is certainly not a problem of the finite element method, but the continuum mechanics model.

An alternative approach to treat material damage nonlocally is to relate the damage evolution with the higher order gradients of the porosity. Ramaswamy and Aravas (1998) suggested a gradient treatment of the porosity of the GTN model. In their study, effects of void diffusion, interaction and coalescence have been considered. Variations of the porosity are characterized by a diffusion equation with a Laplacian of the porosity. The preliminary results of Ramaswamy and Aravas (1998) confirm the mesh-insensitivity in the computational prediction. Due to computational complexity there are no results published on size effects in cracked and notched specimens by using such models.

All those works mentioned above are concentrating on nonlocal treatment of the damage indicator and assuming that the intrinsic material length is only related to damage evolution, which is contradictory to the known experimental observations of significant size effects in plastic deformations of the material matrix by Fleck and Hutchinson (1993, 1997). The strain localization and size effects are not necessarily only related to strain softening. In classical plasticity theory strain softening causes strain localization. In computational modeling the material failure, the strain softening and the strain localization are connected one another. The material damage results in strain softening and the strain softening causes strain localizations. This consideration implies that the true reason for strain localization is the strain softening which can be remedied as shown by de Borst and Mühlhaus (1992). If one corrects the strain localization, one can then predict material failure accurately. On the other hand, it is contradictory to derive a micro-mechanical model within the frame of macro-mechanical theory. If one wants to consider the mechanical processes in microscopic scales, the classical continuum mechanics has to be improved. It has motivated us to embed the micro-mechanical model within a complex continuum theory (Chen and Yuan, 2002; Yuan et al., 2003a).

In the microscopic level we know that the material may show different behaviour, such as the size effect in plastic deformations due to matrix heterogeneity. A logical consequence is to embed the continuum damage model into a plasticity theory frame which has the potential to give a more reliable description of the plastic deformations. In our previous works (Chen and Yuan, 2002; Yuan et al., 2003a) we suggested a modified GTN model coupled with the gradient plasticity, in which the Aifantis' gradient plasticity model is used to describe the matrix behaviour. Introducing gradients of plastic strain into the constitutive model makes material deformations and failure related to the vicinity of the material point. The matrix behaviour is related with the micro-mechanical property by introducing an intrinsic material length. The material damage model becomes nonlocal due to the gradient-dependent constitutive description of the matrix. Numerical examples show that using the finite element formulation the mesh-dependence of damage localization is remedied (Chen et al., 2002). The intrinsic material length in the gradient plasticity may have the potential to predict size effects in material failure (Yuan et al., 2003a,b).

In the present paper we are using both cell element model with constant element length (Sun and Hönig, 1994; Xia and Shih, 1995) and the strain gradient-dependent damage model (Chen and Yuan, 2002; Yuan et al., 2003a) to predict and to analyze the size effect in a German reactor steel 20MnMoNi55. The experimental results (Krompholz et al., 2000b) of notched tension specimens are taken as the reference for comparison. With respect to the experimental records we attempt to give a quantitative comparison between two models.

2. Damage models

In this section we review the known damage model (GTN model) of Gurson (1977), Tvergaard and Needleman (1984) and introduce a nonlocal variety of the GTN model within the frame of the gradient plasticity theory. Attentions are paid to the finite element formulation of the nonlocal damage model.

2.1. The damage model after Gurson, Tvergaard and Needleman (GTN model)

It is generally assumed that the damage of ductile materials begins from micro-voids and defects which are induced due to, e.g., second phase articles in matrices. Based on analysis of a single cell containing a central spherical void in a J_2 elastic–perfectly plastic solid, Gurson (1977) proposed a micro-mechanical constitutive model which describes growth and coalescence of micro-voids in a ductile damage process. This model has been further modified by Tvergaard and Needleman (1984), so that the interaction of micro-voids as well as damage acceleration due to voids coalescence are considered. The yield function of the modified micro-mechanical damage model is expressed as

$$\Phi(q,p,f,\sigma_y)=\frac{q^2}{\sigma_y^2}+2q_1 f\cosh\left(\frac{3q_2p}{2\sigma_y}\right)-(1+q_1^2f^2)=0, \tag{1}$$

where the constants q_1 and q_2 are introduced by Tvergaard and Needleman (1984) to improve predictions of the model for a periodically distributed void array. p and q are the hydrostatic stress and the effective stress of the average macroscopic Cauchy stress $\boldsymbol{\sigma}$ respectively. σ_y is yield stress of the matrix material, and f is the void volume fraction, i.e. the porosity. The evolution equation for the void volume fraction consists of both voids nucleation and growth,

$$\dot{f}=\dot{f}_{\text{growth}}+\dot{f}_{\text{nucleation}}. \tag{2}$$

The void growth is described by incompressibility of plastic deformations

$$\dot{f}_{\text{growth}}=(1-f)\dot{\varepsilon}^{\text{p}}_{kk}, \tag{3}$$

where $\dot{\varepsilon}^{\text{p}}_{ij}$ is the plastic strain rate tensor. A strain-controlled nucleation law is suggested by Chu and Needleman (1980) as

$$\dot{f}_{\text{nucleation}}=\mathscr{A}\dot{\bar{\varepsilon}}^{\text{p}}, \tag{4}$$

where the parameter $\mathscr{A}$ is chosen so that the nucleation strain follows a normal distribution with the mean value ε_N and the standard deviation S_N. $\mathscr{A}$ can be expressed as:

$$\mathscr{A}=\frac{f_N}{S_N\sqrt{2\pi}}\exp\left[-\frac{1}{2}\left(\frac{\bar{\varepsilon}^{\text{p}}-\varepsilon_N}{S_N}\right)^2\right], \tag{5}$$

where f_N is the volume fraction of void nucleating particles. Based on assumption of the plastic flow normality, the macroscopic plastic strain increment is evaluated from

$$\dot{\boldsymbol{\epsilon}}^{\text{p}}=\dot{\lambda}\frac{\partial\Phi}{\partial\boldsymbol{\sigma}}. \tag{6}$$

The equivalent plastic strain $\bar{\varepsilon}^{\text{p}}$ of the matrix material is assumed to vary according to the equivalent plastic work expression,

$$(1-f)\sigma_y\dot{\bar{\varepsilon}}^{\text{p}}=\boldsymbol{\sigma}\dot{\boldsymbol{\epsilon}}^{\mathbf{p}}=\boldsymbol{\sigma}\frac{\partial\Phi}{\partial\boldsymbol{\sigma}}\dot{\lambda}. \tag{7}$$

The matrix material is assumed to satisfy the von Mises yield condition. If $f=0$, this condition becomes the conventional von Mises plasticity with λ as the plastic multiplier.

2.2. A nonlocal damage model under the gradient plasticity

In the GTN model one only considers that the material failure process is modeled by nucleation, growth and coalescence of the micro-voids. The matrix at mesoscopic level is treated as a macroscopic continuum using conventional continuum constitutive relations. Comparing with the known experimental observation (Fleck and Hutchinson, 1993, 2001), it is an obvious shortcoming in this model (Hutchinson, 2000).

According to recent knowledge, the matrix at microscopic level may have different mechanical properties from those at the macroscopic dimensions. Strain gradients may significantly change the matrix strength (Fleck and Hutchinson, 2001). Discussions on the intrinsic material length make it necessary to introduce a material length into the constitutive equation of the matrix. From this background we postulate the matrix strength depending on the strain gradients. According to the known results of de Borst and Mühlhaus (1992) the gradient plasticity has the potential to give a more accurate description of the microscopic

material behaviour (Fleck and Hutchinson, 1993, 2001). In the frame of gradient plasticity suggested by Aifantis (1987), actual flow stress under multi-axial state depends on both plastic strain and it gradients, i.e.

$$\sigma_y(\bar{\varepsilon}^p, \nabla^2\bar{\varepsilon}^p) = \bar{\sigma}(\bar{\varepsilon}^p) - g\nabla^2\bar{\varepsilon}^p, \tag{8}$$

where $\bar{\sigma}(\bar{\varepsilon}^p)$ denotes the yield stress measured in uniaxial tensile tests and g is a positive coefficient with the dimension of force. In this paper, g is assumed as $g = \sigma_0 l^2$ with σ_0 as the initial yield stress and l as an intrinsic material length characterizing micro-structures of the material. If the matrix can be described by the gradient plasticity, we re-write the yield function of the GTN model as

$$\Phi(q, p, f, \sigma_y) = \frac{q^2}{\sigma_y^2(\bar{\varepsilon}^p, \nabla^2\bar{\varepsilon}^p)} + 2q_1 f \cosh\left(\frac{3q_2 p}{2\sigma_y(\bar{\varepsilon}^p, \nabla^2\bar{\varepsilon}^p)}\right) - (1 + q_1^2 f^2) = 0. \tag{9}$$

In the equation above the actual yield stress of the matrix, $\sigma_y(\bar{\varepsilon}^p, \nabla^2\bar{\varepsilon}^p)$, is a function of both equivalent plastic strain and it gradients, represented by $\nabla^2\bar{\varepsilon}^p$. Should material failure be accompanied by high plastic strain gradients, e.g. near a crack tip, the matrix will be substantially strengthened by the gradient term, to prevent strain localization. Such consideration is consistent to the known experimental observations in composite materials (Fleck and Hutchinson, 1993).

2.3. A finite element algorithm for the nonlocal damage model

There are many efficient computational algorithms for the GTN model and some of them have been implemented in the commercial finite element code (ABAQUS, 2001). The cell model uses the standard algorithm for computations originally suggested by Aravas (1987). The integration algorithm for the GTM model has been implemented into the ABAQUS code using the user interface UMAT. Details of the implementation are described in ABAQUS (2001) and Aravas (1987) and will not repeat in this paper. In the following we just review the finite element formulation of the nonlocal GTN model suggested in the previous section. More details of the algorithm have been reported by Chen and Yuan (2002) as well as by Yuan et al. (2003a).

Due to the higher order differentiation of the equivalent plastic strain $\bar{\varepsilon}^p$, the conventional finite element technique based on the C^0 interpolation (Zienkiewicz, 1971) becomes inapplicable. A robust computational algorithm is essential for validation and application of such complex constitutive model.

Let V and V^p denote the volume occupied by the body and its plastic part, respectively. S denotes the surface bounding the volume V and S^p is the elastic–plastic boundary surface of V^p, $\boldsymbol{n}$ the normal vector of the elastic–plastic boundary surface S^p. Following Mühlhaus and Aifantis (1991) as well as de Borst and Mühlhaus (1992), the generalized variational about the deformation rate $\boldsymbol{v}$ and λ can be expressed as

$$\delta\Pi(\boldsymbol{\sigma}, \bar{\varepsilon}^p, \delta\boldsymbol{v}, \delta\dot{\lambda}) = \int_V \boldsymbol{\sigma}\nabla\,\delta\boldsymbol{v}\,\mathrm{d}V + \int_S \bar{\boldsymbol{t}}\,\delta\boldsymbol{v}\,\mathrm{d}S + \int_{V^p} \Phi(q, p, f, \sigma_y(\bar{\varepsilon}^p, \nabla^2\bar{\varepsilon}^p))\delta\dot{\lambda}\,\mathrm{d}V + \int_{S^p} \frac{\partial\bar{\varepsilon}^p}{\partial\boldsymbol{n}}\delta\dot{\lambda}\,\mathrm{d}\boldsymbol{S}. \tag{10}$$

The solution is obtained as soon as the generalized variational $\delta\Pi$ vanishes,

$$\delta\Pi(\boldsymbol{\sigma}, \bar{\varepsilon}^p, \delta\boldsymbol{v}, \delta\dot{\lambda}) = 0. \tag{11}$$

Neglecting body forces follows two basic weak form equations as

$$\int_V \delta\boldsymbol{v}\nabla\boldsymbol{\sigma}\,\mathrm{d}V = 0, \tag{12}$$

$$\int_V \delta\dot{\lambda}\Phi(q, p, f, \sigma_y(\bar{\varepsilon}^p, \nabla^2\bar{\varepsilon}^p))\,\mathrm{d}V = 0 \tag{13}$$

with an additional boundary condition $\partial\bar{\varepsilon}^{\mathrm{p}}/\partial \boldsymbol{n} = 0$ on the plastic border V_{p}. The equations above are fundamental in the finite element method for the gradient plasticity theory. Note we take the total stress and total plastic strain in the integrand which is equivalent to the rate variational equation by de Borst and Mühlhaus (1992) and Mühlhaus and Aifantis (1991) under infinitesimal displacement assumptions.

Due to the complicated constitutive relation between the plastic multiplier λ and effective plastic strain $\bar{\varepsilon}^{\mathrm{p}}$ in Eq. (9), we have to discretise Eq. (7) as the third governing equation for the finite element formulation,

$$\int_V \delta\dot{\bar{\varepsilon}}^{\mathrm{p}} \left[(1-f)\sigma_{\mathrm{y}}\dot{\bar{\varepsilon}}^{\mathrm{p}} - \boldsymbol{\sigma}\frac{\partial \Phi}{\partial \boldsymbol{\sigma}}\dot{\lambda} \right] \mathrm{d}V = 0. \tag{14}$$

The variational equations (12)–(14) build the fundamental of the finite element algorithm for the nonlocal micro-mechanical damage model within the gradient plasticity.

The basic unknown variables in the equations are the displacement vector (Zienkiewicz, 1971), $\boldsymbol{u}$, the equivalent plastic strain $\bar{\varepsilon}^{\mathrm{p}}$ as well as the plastic multiplier λ, as shown in Fig. 1. The integral expressions will be converted into algebraic equations by using suitable interpolation functions. We take the following interpolations for the field variables

$$\boldsymbol{u}(\boldsymbol{x}) = [\boldsymbol{N}(\boldsymbol{x})]\boldsymbol{u}_{\mathrm{node}}, \tag{15}$$

$$\lambda(\mathbf{x}) = [\boldsymbol{N}_{\mathbf{1}}(\boldsymbol{x})]\boldsymbol{\Lambda}_{\mathrm{internal}}, \tag{16}$$

$$\bar{\varepsilon}^{\mathrm{p}}(\mathbf{x}) = [\boldsymbol{H}(\boldsymbol{x})]\boldsymbol{\Upsilon}_{\mathrm{node}}, \tag{17}$$

where $[\boldsymbol{N}(\boldsymbol{x})]$ is the standard 8-nodal serendipity interpolation function for displacement, $[\boldsymbol{H}(\boldsymbol{x})]$ is the C^1-continuous implicit Hermitian interpolation function for plastic strain, which has been discussed in detail separately (Chen and Yuan, 2002; Yuan and Chen, 2002a,b). $[\boldsymbol{N}_{\mathbf{1}}(\boldsymbol{x})]$ is the interpolation function for the plastic multiplier. Details of the present algorithm are reported in our previous paper on the computational algorithm (Chen and Yuan, 2002).

Considering finite strain assumptions, the equilibrium equation (12) at the current configuration can be simply written as (ABAQUS, 2001)

$$\int_V \boldsymbol{\sigma}\,\delta\nabla\boldsymbol{v}\,\mathrm{d}V = 0. \tag{18}$$

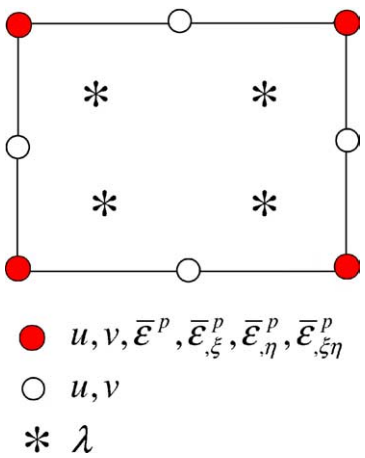

Fig. 1. The C^1 element with λ as internal nodes introduced for nonlocal damage model.

To solve the nonlinear differential integro-equation, one uses the Newton iteration method. Setting $\boldsymbol{\sigma} = \boldsymbol{\sigma}^0 + \dot{\boldsymbol{\sigma}}\,\mathrm{d}t$, the equation above can be converted into

$$\int_V \dot{\boldsymbol{\sigma}}\,\delta\nabla\boldsymbol{v}\,\mathrm{d}t\,\mathrm{d}V = \delta\overline{F} \tag{19}$$

with the residuum force in the spatial coordinates

$$\delta\overline{F} = -\int_V \boldsymbol{\sigma}^0\,\delta\nabla\boldsymbol{v}\,\mathrm{d}V. \tag{20}$$

In the expression $\boldsymbol{\sigma}^0$ stands for total stress tensor of the last increment step in the current configuration. $\dot{\boldsymbol{\sigma}}$ is the rate of Cauchy stress tensor and $\nabla\boldsymbol{v}$ denotes the gradient of the deformation rate. The objective stress rate at the current configuration, the Jaumann stress rate, $\boldsymbol{\sigma}^*$, which is suitable in the constitutive relation, is defined in ABAQUS (2001)

$$\boldsymbol{\sigma}^* = \dot{\boldsymbol{\sigma}} + \boldsymbol{\sigma}\cdot\boldsymbol{D} + \boldsymbol{D}\cdot\boldsymbol{\sigma} - \boldsymbol{\sigma}\cdot\nabla\boldsymbol{v} - \nabla\boldsymbol{v}\cdot\boldsymbol{\sigma} \tag{21}$$

with the strain rate tensor

$$\boldsymbol{D} = \tfrac{1}{2}(\nabla\boldsymbol{v} + \boldsymbol{v}\nabla). \tag{22}$$

Then Eq. (19) becomes (ABAQUS, 2001)

$$\int_V \left[\boldsymbol{\sigma}^*\,\delta\boldsymbol{D} - \frac{1}{2}\boldsymbol{\sigma}\,\delta(2\boldsymbol{D}\boldsymbol{D}^{\mathrm{T}} - \nabla\boldsymbol{v}\cdot\boldsymbol{v}\nabla)\right]\mathrm{d}V = \delta\overline{F}. \tag{23}$$

Substituting Eqs. (15)–(17) into (23), (13), (14), the governing equations can be re-written as

$$\int_V \boldsymbol{B}^{\mathrm{T}}\boldsymbol{\sigma}^* + \boldsymbol{\sigma}\left[\left(\frac{\partial\boldsymbol{N}}{\partial\boldsymbol{x}}\right)^{\mathrm{T}}\frac{\partial\boldsymbol{N}}{\partial\boldsymbol{x}} - 2\boldsymbol{B}^{\mathrm{T}}\boldsymbol{B}\right]\mathrm{d}V = \boldsymbol{F}_\sigma, \tag{24}$$

$$\int_V \boldsymbol{N}_1^{\mathrm{T}}\left(\frac{\partial\Phi}{\partial\boldsymbol{\sigma}}\dot{\boldsymbol{\sigma}} + \frac{\partial\Phi}{\partial\sigma_{\mathrm{y}}}\dot{\sigma}_{\mathrm{y}} + \frac{\partial\Phi}{\partial f}\dot{f}\right)\mathrm{d}V = \boldsymbol{F}_\varepsilon, \tag{25}$$

$$\int_V \boldsymbol{H}^{\mathrm{T}}\left[(1-f)\sigma_{\mathrm{y}}\dot{\bar{\varepsilon}}^{\mathrm{p}} - \dot{\lambda}\boldsymbol{\sigma}\frac{\partial\Phi}{\partial\boldsymbol{\sigma}}\right]\mathrm{d}V = 0. \tag{26}$$

In equations above $\boldsymbol{B}$ is the strain–displacement relation matrix. The last parentheses in (24) are the part of geometric stiffness matrix (ABAQUS, 2001). Eq. (25) is derived from the weak form of the yield condition (13) by differentiating the potential function about $\boldsymbol{\sigma}$, σ_{y} and f. The residuum forces are expressed by

$$\boldsymbol{F}_\sigma = -\int_V \boldsymbol{B}^{\mathrm{T}}\boldsymbol{\sigma}^0\,\mathrm{d}V, \tag{27}$$

$$\boldsymbol{F}_\varepsilon = -\int_V \boldsymbol{N}_1^{\mathrm{T}}\boldsymbol{\Phi}^0\,\mathrm{d}V \tag{28}$$

with $\boldsymbol{\Phi}^0$ as the residuum of the yield function $\boldsymbol{\Phi}$ from the last iteration step.

The plastic multiplier λ is treated as an internal variable in the finite element formulation which will be solved for each element. On the other hand, during plastic loading and unloading, the Kuhn–Tucker conditions

$$\dot{\lambda} \geqslant 0; \quad \Phi(\bar{\varepsilon}^{\mathrm{p}}, \nabla^2\bar{\varepsilon}^{\mathrm{p}}) \leqslant 0; \quad \dot{\lambda}\Phi(\bar{\varepsilon}^{\mathrm{p}}, \nabla^2\bar{\varepsilon}^{\mathrm{p}}) = 0 \tag{29}$$

must be fulfilled in each Gauss integration point. Since the yield condition is enforced for an element globally, care should be taken in the numerical handling.

The plastic multiplier vector $\boldsymbol{\Lambda}_{\text{internal}}$ denotes the value of λ on the four Gauss points of each element (Fig. 1). It is an internal vector of an element. At the Gauss points, if $\Phi < 0$, the Gauss point is elastic and $\dot{\lambda}$ is forced to zero. It follows that the second governing equation becomes trivial. On the other case, if $\Phi > 0$, the point is judged to plastic and the governing equation $\int_V \boldsymbol{N}_1^T \Phi(\bar{\varepsilon}^{\mathrm{p}}, \nabla^2 \bar{\varepsilon}^{\mathrm{p}})\,\mathrm{d}V = 0$ has to be satisfied. The condition $\dot{\lambda}\Phi(\bar{\varepsilon}^{\mathrm{p}}, \nabla^2 \bar{\varepsilon}^{\mathrm{p}}) = 0$ is achieved at all plastic Gauss points.

In the 8-nodal C^1-continuous Hermitian interpolation, vanishing of the global residual vector, $\int_V \boldsymbol{H}^{\mathrm{T}}[(1-f)\sigma_{\mathrm{y}}\dot{\bar{\boldsymbol{\varepsilon}}}^{\mathrm{p}} - \boldsymbol{\sigma}\,\partial\Phi/\partial\boldsymbol{\sigma}\dot{\lambda}]\,\mathrm{d}V$, follows that the integrand $(1-f)\sigma_{\mathrm{y}}\dot{\bar{\boldsymbol{\varepsilon}}}^{\mathrm{p}} - \boldsymbol{\sigma}\,\partial\Phi/\partial\boldsymbol{\sigma}\dot{\lambda}$ approaches zero at all plastic Gauss points in the element. Thus, the classical Kuhn–Tucker conditions (29) are fulfilled. The integral formulation is equivalent to the discrete condition. The discrete Kuhn–Tucker condition suggested by Ramaswamy and Aravas (1998) can be avoided.

Introducing additional higher order gradients into the governing equations, one needs more boundary conditions to maintain the uniqueness of the solution. Except the conventional displacement and traction boundary conditions, we have to formulate additional boundary conditions for the plastic strains. Mühlhaus and Aifantis (1991) introduced

$$\frac{\partial \bar{\varepsilon}^{\mathrm{p}}}{\partial \boldsymbol{n}} = 0 \tag{30}$$

as the additional boundary condition along the plastic boundary. Additionally, Pamin (1994) suggested

$$\frac{\partial^2 \bar{\varepsilon}^{\mathrm{p}}}{\partial \boldsymbol{n}\partial \boldsymbol{m}} = 0 \tag{31}$$

to suppress the system singularity. In the equation above $\boldsymbol{n}$ and $\boldsymbol{m}$ denote the normal and tangent vector of the plastic boundary, respectively. Since we introduce terms with the second order of differentiation into the constitutive equation, the two independent conditions will maintain the uniqueness of the plasticity solution. According to analysis of Pamin (1994) this condition assures the correct rank of the stiffness matrix. Frankly speaking, these boundary conditions are rather artificial from the point of view of continuum mechanics. Whereas (31) is a direct consequence of (30), Eq. (30) itself requires a smooth diminishing of the equivalent plastic strain to the elastic zone. If the plastic zone is bounded by the specimen boundary, however, such boundary condition could be over-restrained. It remains an open issue within the gradient plasticity for more detailed analysis of the constitutive equations.

3. Constitutive parameters

Material damage in a German reactor pressure vessel steel, 20 MnMoNi55, is considered. Extensive experiments have been conducted within a European research program (Krompholz et al., 2000a,b). Different scaled, geometry-similar specimens are tested and documented. In this work the experimental records are taken as reference to examine computational predictions based on both conventional GTN damage model and nonlocal damage model.

It is usual that the stress–strain curve is taken from uniaxial tension tests. In such process one assumes that the experimental records are not affected by the specimen size, provided that the material is homogeneous. To identify the parameters of elastic-plasticity behaviour we only use the data up to the stress maximum points from uniaxial tension tests. Beyond the ultimate stress point the specimen deformations are affected by material damage substantially. For computations, the stress–strain curve beyond the ultimate stress point is extrapolated using the same power-law with a unique strain hardening exponent. According to our fitting the material parameters are set as following: Young's modulus $E = 500\sigma_0$, the

initial yield stress $\sigma_0 = 435$ MPa, the strain hardening exponent $n = 7.25$. The uniaxial stress–strain relation can be expressed as

$$\sigma = \begin{cases} E\varepsilon & 0 \leqslant \varepsilon \leqslant 0.002; \\ \sigma_0 & 0.002 < \varepsilon \leqslant 0.01; \\ \alpha\sigma_0(\varepsilon - \varepsilon_0)^{(1/n)} & \varepsilon > 0.01. \end{cases} \tag{32}$$

with $\varepsilon_0 = 0.0087$, $\alpha = 2.5$ is a fitting parameter. The power-law above is plotted together with the experimental results in Fig. 2. Up to the over-proportional increasing of the true stress due to high stress triaxiality and necking, the supposed stress–strain relation fits the experimental record well.

For identifying the material parameters in the GTN damage model, we need the experimental records beyond the ultimate stress point. Generally speaking, we can neglect size effects in the largest specimen to find out the best fit. As discussed by Yuan et al. (2003a) the element size does not affect the prediction of material failure in uniaxial tensile specimens. It implies that we may identify parameters in the GTN model from any uniaxial experiment using an arbitrarily fine mesh.

From analysis of the GTN model we know the parameters $q_1 = 1.5$ and $q_2 = 1$ for ductile materials. Assuming the initial porosity will change the maximum stress level in the uniaxial tension simulation. We set $f_0 = 0.001$ and without void nucleation $f_N = 0$. The critical porosity describes coalescence of voids and characterizes the instable point in the uniaxial tension tests. $f_c = 0.01$ gives us a reasonable prediction in all tension specimens.

To consider rapid expansion of voids beyond the critical porosity f_c, Tvergaard and Needleman (1984) introduced bi-linear extrapolation of the porosity in the constitutive equation (1), that is, the void volume function f in Eq. (1) is replace by f^* defined as

$$f^* = \begin{cases} f & \text{if } f \leqslant f_c; \\ f_c + K(f - f_c) & \text{if } f \geqslant f_c, \end{cases} \tag{33}$$

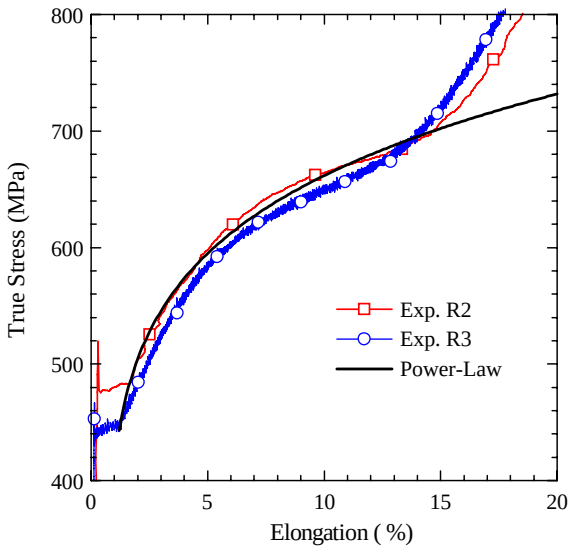

Fig. 2. Stress–strain relation measured in the uniaxial tension specimens at room temperature as well as the stress–strain curve used for computations. The stress versus plastic strain relation is assumed in a power-law function form with the strain-hardening exponent $n = 7.25$.

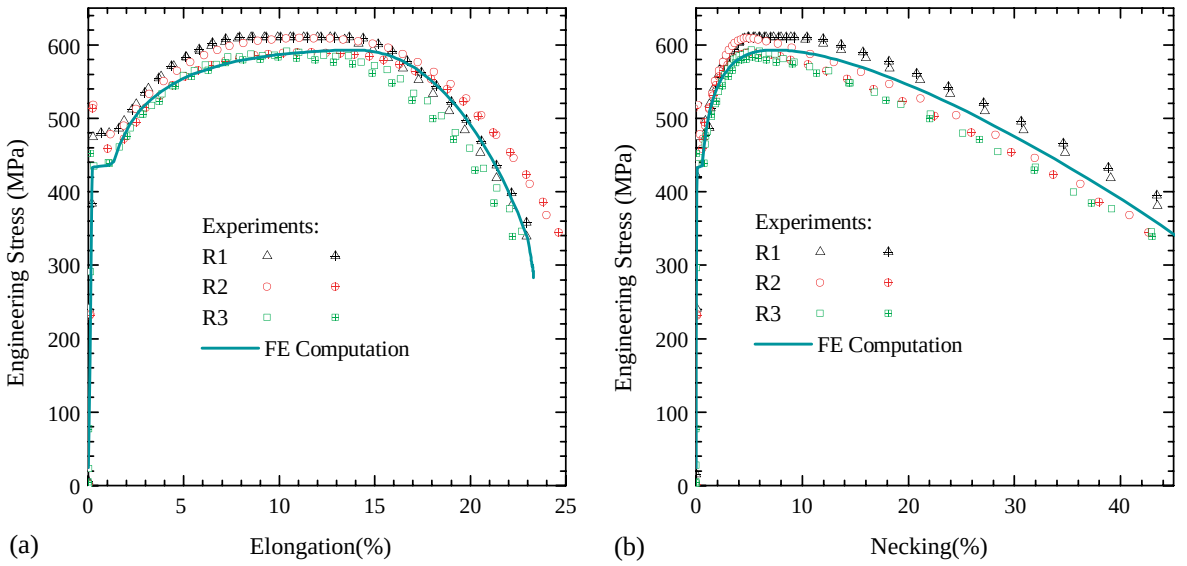

Fig. 3. Comparison between the experimental and computational results of *the smooth tensile specimens*. The diameters of the specimens are 3, 9 and 30 mm, respectively. The computations are conducted using the nonlocal damage model with a length scale parameter $l = 0.24$ mm.

with $K = 3$ as an additional damage parameter. To prevent numerical difficulty after material failure, the final flow stress is limited to ten percent of the initial yield stress after void coalescence. It means the material does not lose whole loading capacity.

Identifying the material length parameter is a special task in the present nonlocal damage. From discussion by Yuan and Chen (2000, 2002a,b) the material length is related to plastic deformations and describes localized plastic deformations. The parameter can be determined from the micro-indentation tests. For the present material the micro-indentation tests have not been performed. The material length will be determined based on numerical experiments. Summarizing the simulations of different specimens we find the material length should be between 0.2–0.3 mm. In our computational investigations presented in the following section we set $l = 0.24$ mm. The computational results are plotted in Fig. 3 together with the experimental records. In the figure R1, R2 and R3 denote different sized specimens. R3 is ten times as large as R1.

The finite element width in the cell model cannot be found from the uniaxial tension. Usually one determines this length from notched or cracked specimens to fit the experimental result (Brocks et al., 1995; Sun and Hönig, 1994; Xia and Shih, 1995). In this work we have varied the element length systematically and to show the effects in predicting specimen load capacity in the next section.

4. Results for notched specimens

To investigate the size effect three different sized specimens have been tested by Krompholz et al. (2000b). The specimen geometry is plotted in Fig. 4. Three specimens are scaled by factor 1, 3 and 10, which are termed T1, T2 and T3, respectively. Should there be no size effects, nondimensionalized experimental results will fall into a single curve. In experiments both local and global displacements have been measured. It is observed that the local displacements around the notch vary with the specimen size (Krompholz et al.,

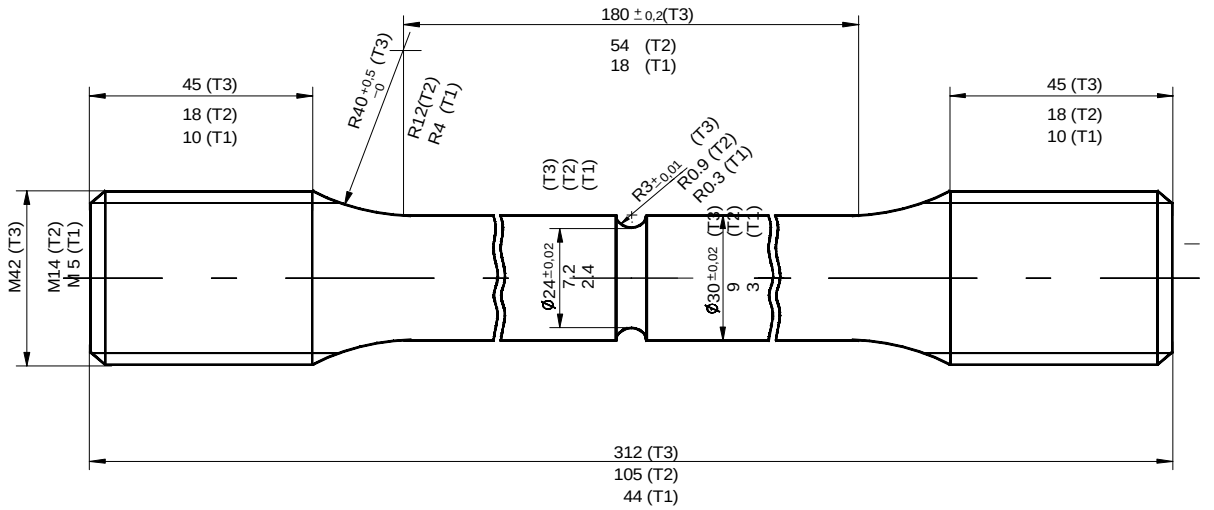

Fig. 4. Geometry of *notched tension specimens* (Krompholz et al., 2000b). Three different sizes are considered. The specimens are made of a reactor pressure vessel steel 20MnMoNi55. The scale factors are 1, 3 and 10, respectively.

2000b). The displacements in the largest specimen are stronger concentrated to the notch. The small specimen shows a smoother displacement variation.

In computations using the cell model we set the element size near to the notch to 0.3 mm × 0.5 mm. Since the element size is the same for all three specimens, it follows that the smallest specimen T1 only has 4 elements in the symmetric ligament. Generally speaking a coarser element mesh will arise the load capacity of the specimen slightly. This effect can be observed in the following discussions. For three specimen we vary the mesh proportionally so that the element size for all specimens remains the same. It has been shown that further variations of the element size will not substantially change computational results for the present work.

For the nonlocal damage model the element size is, generally speaking, insignificant to the computational results which has been confirmed based on extensive computational verifications (Chen and Yuan, 2002; Yuan et al., 2003a). The Laplacian term in the effective yield stress evaluation remedies the dependence on the numerical discretization even when the material displays strong instable behaviour.

For comparison purpose the computational results from both cell model and nonlocal damage model are plotted together with the corresponding experimental records. In Fig. 5 the mean stress defined as the traction divided by the initial cross area of the specimen is shown as a function of the axial elongation. There are two experimental records plotted in the figure. In the research program of Krompholz et al. (2000b) much more specimens have been tested. The two representative experimental records stand for the scattering borders of the material properties. It is obvious that the same material scattering will change the mean stress curves of the small specimens more significantly than those of the large ones.

From the figures one may see that for the same scaled elongation the mean stress of the smallest specimen T1 is significantly larger than that in the other specimens T2 and T3. T1 also reaches higher ultimate stress. Specimens T2 and T3 do not display obvious influence of the specimen size. This experimental observation can be modeled using the nonlocal damage model very well as shown in the mean stress versus elongation curves (Fig. 5(b)), but not the cell model (Fig. 5(a)) using the conventional GTN equation (1). In the mean stress versus necking curves the effect from averaging the porosity in the cell model seems too weak to change the global traction. Only in the instable fracture phase the T1 in the cell model shows

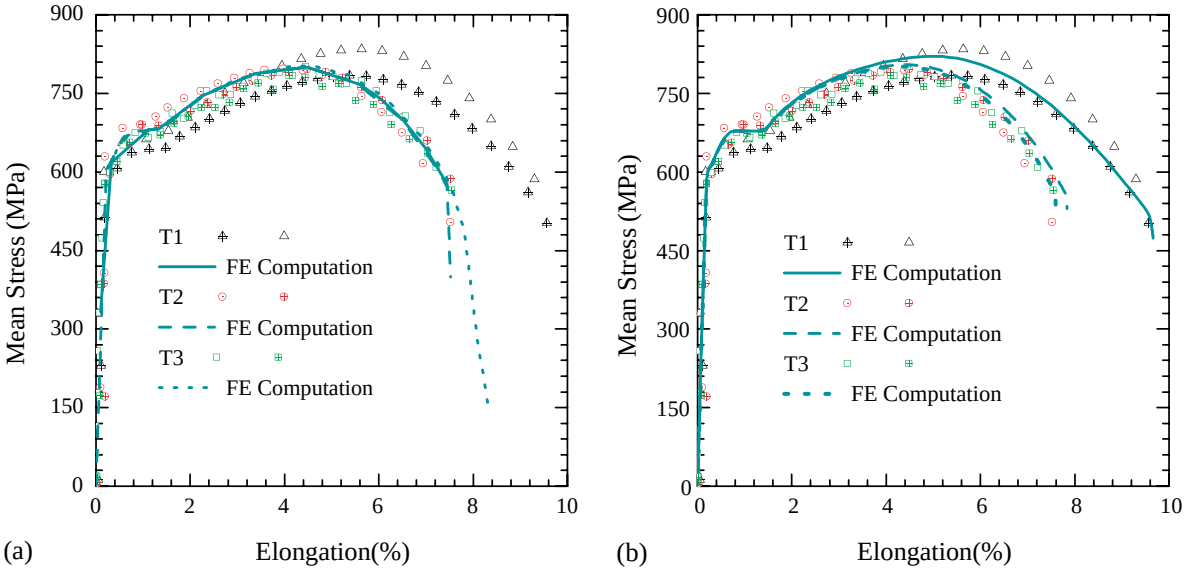

Fig. 5. Comparison between the experimental and computational results for the notched specimens: The nominal tension stress versus elongation. (a) Cell model results. (b) Computations of the nonlocal damage model with $l = 0.24$ mm.

slightly higher strength than the larger specimens. In the nonlocal computations the iterations fail to converge for instable crack propagation.

Fig. 6 shows, furthermore, a good agreement in elongation versus necking relations for the large specimens using both computational models. In small necking region the experimental records contain rather large scattering, where the size effects are not essential, and at large displacements the computational curves reproduce experimental measurements very well. The smallest notched specimen displays significantly higher loading capacity than the others do. This feature can be clearly identified in the nonlocal model computation, but not in the cell model. The similar results are plotted in Fig. 7 in which the elongation is shown as a function of the necking.

The reason for such results can be found in variations of the equivalent plastic strains which are summarized in Figs. 8 and 9. For both models we use the reduced integration technique in the finite element method (ABAQUS, 2001). It follows that the distribution of the equivalent plastic strain within an element is a linear function of the location. For the smallest specimen T1 in the cell model (Fig. 8) only four equal-sized elements have been used in the radial direction, whereas T3 has forty elements. It follows significantly different distribution due to the different numerical descritizations. Originally one hopes that the coarse element with linear plastic strain distribution may eliminate the strain localization and so reaches the certain crack initiation load. From Fig. 8 one may say that such a delay in material failure is rather artificial and depends substantially on the strain gradient variation, that is, on the notch geometry and the load configuration. In our case the amplitudes of the porosity in both specimens are in the same level so that the further evolution of the material damage is not affected by the specimen size. Therefore, one does not see effects of the element size, i.e. the element size does not happen to fit the expected delay of the crack initiation and the size effect can not predicted by the cell model.

In Fig. 9 development of the porosity from the nonlocal damage model is summarized. In the figure the porosity is expressed as a function of the normalized specimen radius R/R_0. The distribution is smoothed due to the C^1 interpolation. It is to see that for the same elongation the damage zone concentrates strongly in the center of the large specimen and the material loses its load capacity in the specimen center quickly. In

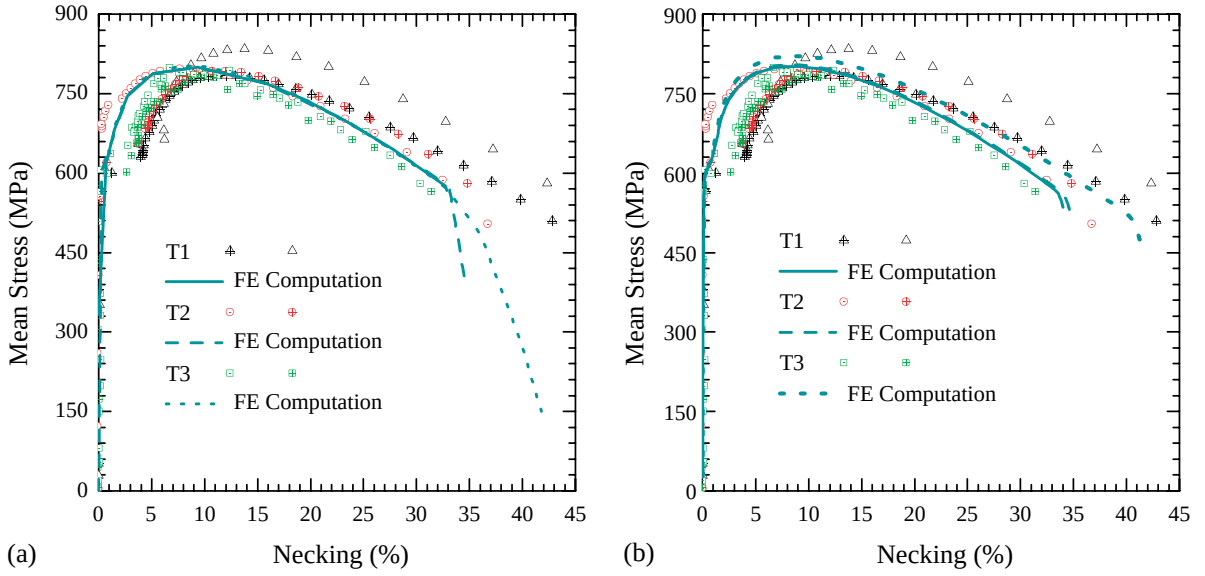

Fig. 6. Comparison between the experimental and computational results for the notched specimens: The nominal tension stress versus Necking. (a) Cell model results. (b) Computations of the nonlocal damage model with $l = 0.24$ mm.

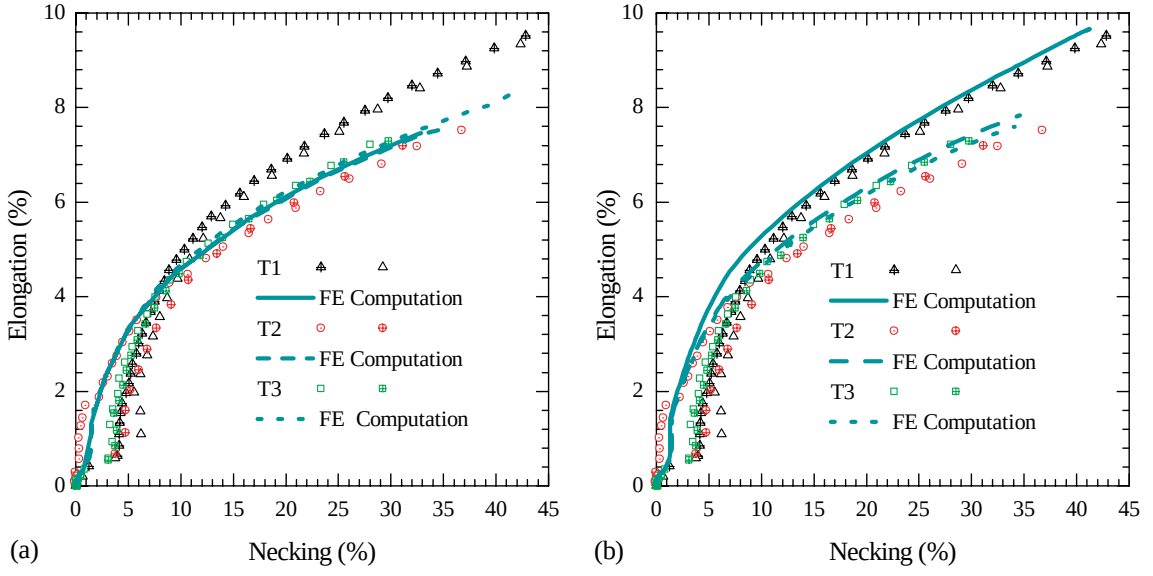

Fig. 7. Elongation as a function of the side nicking in the notched tension specimens. (a) Cell model results. (b) Computations of the nonlocal damage model with $l = 0.24$ mm.

the smallest specimen T1 the distribution of the porosity is more homogeneous in the radial direction due to effects of the material length l than T3. l affects evolution of plastic strains and so the porosity. It follows that the material failure begins earlier in T3 than that in T1. In a nondimensionalized diagram the small

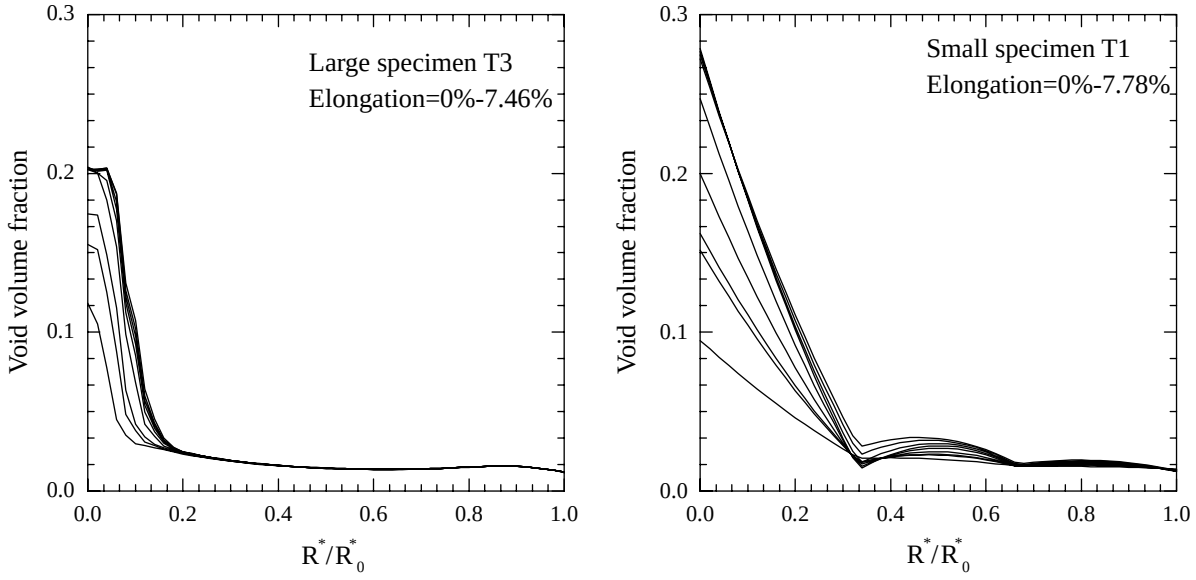

Fig. 8. Variations of the porosity in the notched tension specimens using the GTN model with constant element size (the cell model). The horizontal axis is normalized by the initial diameter of the specimens.

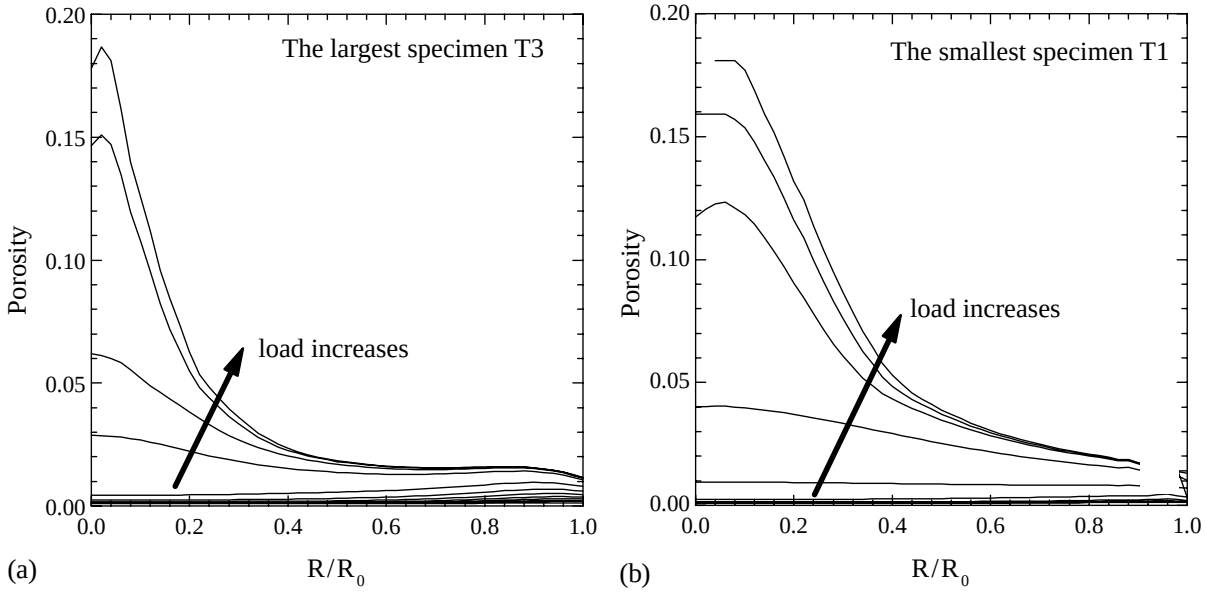

Fig. 9. Variations of the porosity in the notched tension specimens using the nonlocal damage model with $l = 0.24$ mm. The horizontal axis is normalized by the initial diameter of the specimens.

specimen has higher loading capacity than the large one. In plastic deformations we see that the smallest specimen contains much more plastic energy in a unit volume than in the large specimen, it delays pro-

pagation of the damage zone. This observation gives an understandable explanation of the size effect in the present experiments.

In the nonlocal model variations of the plastic strain are controlled by the material length introduced for the gradient plasticity. The plastic strain distribution is independent of the finite element mesh. The numerical integration and descritization are features of the mathematical approximation method. Shortcoming in a constitutive model cannot be compensated by changing computational accuracy.

In the GTN model the porosity distributes similarly to the plastic strain which is given by the constitutive equation. The porosity from the nonlocal damage model, however, is affected by the absolute specimen size, that is, the ratio of the specimen size to the material length. It makes the prediction of the specimen failure varies with the specimen size. By changing the scaling factor of the notched tensile specimens we may obtain systematic variations of the loading capacity of the specimen. Using the nonlocal model we are able to give a computational prediction of the size-dependent material failure.

Based on extensive computations of the various scaling factors, we can show that there is a general relation between the size effect and the material length parameter as

$$U = U_0\left(1 + \frac{\kappa l^2}{D^2}\right), \tag{34}$$

where U denotes a characteristic deformation at specimen fracture, e.g. notch opening displacement, necking etc. U_0 represents the characteristic displacement in the same kind of notched tension specimens without size effects, i.e. $l \approx 0$. κ is a geometric factor of the characteristic displacement. For the notch opening displacement κ is about 1. This equation is verified based on numerous finite element computations using different l values, as shown in Fig. 10.

This expression is of great interesting for predict size effects in ductile materials and valid for the local displacement with significant plastic deformations. It generally means that for a given material, i.e. for a given l, the local displacements at material failure depend on inverse of square of the characteristic specimen size, that is,

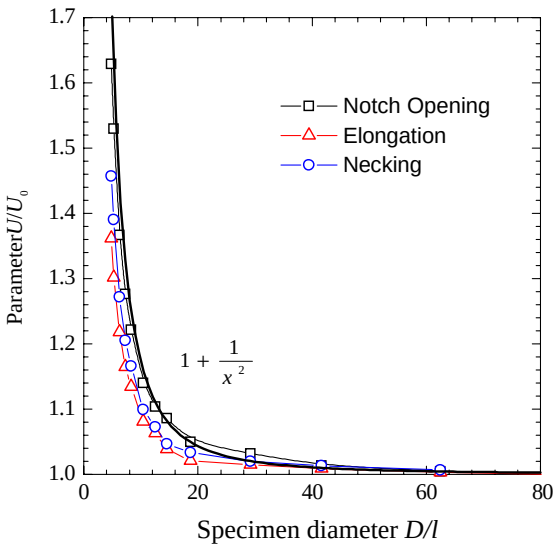

Fig. 10. Effects of the round notched tension specimen size. The computational results of the notch opening displacement, elongation and necking are normalized by the values with $l = 0$. The specimen diameter is nondimensionalized by the material length l.

$$U = \mathrm{O}\left(\frac{l^2}{D^2}\right). \tag{35}$$

From a given specimen one may extrapolate the displacement for any other sized specimen.

Furthermore, one may image to relate this relation with general fracture criterion. From fracture mechanics we know that the crack tip opening displacement (CTOD) is linearly correlated with the J-integral. Using the relation (34) one may image

$$J = J_0\left(1 + \frac{\kappa l^2}{a^2}\right), \tag{36}$$

where J_0 denotes a critical value in a reference specimen and a a characteristic size of the specimen to be considered. Should Eq. (36) be valid for the crack specimen, the size effect can be analytically integrated into the J-integral criterion directly. To finalize this concept more extensive researches are necessary.

5. Conclusions

Systematic experimental results confirm material failure displays significant size effects which are related to strain gradients. The smallest notched specimen possesses significantly higher nondimensionalized loading capacity than the larger specimens. One may expect more significant deviations in a sharper notched or smaller specimen.

The cell model based on the GTN damage model cannot reproduce the experimental measurements of the smallest specimen. The smoothing strain variations in a damaged element by using constant element size may not induce such strong nonlocal effects in the computation that the global load will be changed. This prediction is not contradictory to the known results. One may image the applicability of the cell model is strongly related to the strain gradient distributions around the damaged zone. For sharp notches or even cracks the smoothing strain variations in a conventional element is more effective than that in weakly notched specimens with low strain gradients. Our examples show averaging the strain distribution within an element may not be enough for a reliable material failure prediction.

The size effect can be caught by the nonlocal damage model modified from the known GTN model. Predictions of specimen failure do not depend on the artificial finite element size. Further variations of the specimen size display that the local displacements at material failure are a square function of the intrinsic material length. The size effect can be observed only if the specimen dimension approaches the order of the material length.

References

ABAQUS User Manual, Version 6.2, Hibbitt, 2001. Karlsson and Sorensen, Inc., Providence, RI.

Aifantis, E.C., 1987. The physics of plastic deformation. International Journal of Plasticity 3, 211–247.

Aravas, N., 1987. On the numerical integration of a class of pressure-dependent plasticity models. International Journal for Numerical Methods in Engineering 24, 1395–1416.

Brocks, W., Hönig, A., Sun, D.-Z., 1995. Verification of the transferability of micromechanical parameters by cell model calculations with visco-plastic materials. International Journal of Plasticity 11, 971–987.

Chen, J., Yuan, H., 2002. A micromechanical damage model based on gradient plasticity: algorithms and applications. International Journal for Numerical Methods in Engineering 54, 199–220.

Chen, J., Yuan, H., Wittmann, F.H., 2002. Computational simulations of micro-indentation tests using gradient plasticity. Computer Modeling in Engineerings and Sciences 3, 743–754.

Chu, C.C., Needleman, A., 1980. Void nucleation effects in biaxially stretched sheets. International Journal of Engineering Materials Technology 102, 249–256.

de Borst, R., Mühlhaus, H., 1992. Gradient-dependent plasticity: formulation and algorithmic aspects. International Journal for Numerical Methods in Engineering 35, 521–539.
Fleck, N.A., Hutchinson, J.W., 1993. A phenomenological theory for strain gradient effects in plasticity. Journal of the Mechanics and Physics of Solids 41, 1825–1857.
Fleck, N.A., Hutchinson, J.W., 1997. Strain gradient plasticity. Advances in Applied Mechanics 33, 295–361.
Fleck, N.A., Hutchinson, J.W., 2001. A reformulation of strain gradient plasticity. Journal of the Mechanics and Physics of Solids 49, 2271–2445.
Gurson, A.L., 1977. Continuum theory of ductile rupture by void nucleation and growth: Part I—yield criteria and flow rules for porous ductile media. Journal of Engineering Materials and Technology 99, 2–15.
Hutchinson, J.W., 2000. Plasticity at the micro scale. International Journal of Solids and Structures 37, 225–239.
Krompholz, K. et al., 2000a. Size effect studies on smooth tensile specimens at room temperature and 400 °C. EU-Research Project: REVISA, Paul Scherrer Institute, June 2000.
Krompholz, K. et al., 2000b. Size effect studies on notched tensile specimens at room temperature and 400 °C. EU-Research Project: REVISA, Paul Scherrer Institute, June 2000.
Leblond, J.B., Perrin, G., Devaux, J., 1994. Bifurcation effects in ductile materials with damage localization. Journal of Applied Mechanics 61, 236–242.
Mühlhaus, H.B., Aifantis, E.C., 1991. A variational principle for gradient plasticity. International Journal of Solids and Structures 28, 845–857.
Pamin, J., 1994. Gradient-dependent plasticity in numerical simulation of localization phenomena. PhD Thesis, Delft University of Technology, 1994.
Ramaswamy, S., Aravas, N., 1998. Finite element implementation of gradient plasticity models—Part I, Part II. Computer Methods in Applied Mechanics and Engineering 163, 33–53.
Sun, D.-Z., Hönig, A., 1994. Significance of the characteristic length for micromechanical modeling of ductile fracture. In: Proc. 3rd Conf. on Localized Damage. Comp. Mech. Publ., Southampton.
Tvergaard, V., 1981. Influence of voids on shear band instabilities under plane strain conditions. International Journal of Fracture 17, 389–407.
Tvergaard, V., Needleman, A., 1984. Analysis of the cup-cone fracture in a round tensile bar. Acta Metallurgica 32, 157–169.
Tvergaard, V., Needleman, A., 1995. Effects of nonlocal damage in porous plastic solids. International Journal of Solids and Structure 32, 1063–1077.
Xia, L., Shih, C.F., 1995. Ductile crack growth—I. Numerical study using computational cells with microstructurally-based length scales. Journal of Mechanics and Physics of Solids 43, 233–259.
Yuan, H., Chen, J., 2000. Analysis of size effects based on a lower-order gradient plasticity model. Computational Material Science 19, 143–157.
Yuan, H., Chen, J., 2002a. Identification of intrinsic material length in gradient plasticity from micro-indentations. International Journal of Solids and Structures 38, 8171–8187.
Yuan, H., Chen, J., 2002b. The role of material internal lengths in micro-indentation tests. Computational Material Science 25, 253–263.
Yuan, H., Chen, J., Krompholz, K., Wittmann, F.K., 2003a. Investigations of size effects in tensile tests based on a nonlocal micromechanical damage model. Computational Material Sciences 26, 230–243.
Yuan, H., Chen, J., 2003b. Computational analysis of the thermal barrier coating systems using a cohesive model and gradient plasticity. Engineering Fracture Mechanics 70, 1929–1942.
Zienkiewicz, O.C., 1971. The Finite Element Method in Engineering Science. McGraw-Hill Publishing Company, London.